

Spatial Coherence of a Polariton Condensate

Hui Deng^{1*}, Glenn S. Solomon² Rudolf Hey³, Klaus H. Ploog³, Yoshihisa Yamamoto^{1,4}

¹*Edward L. Ginzton Laboratory, Stanford University, Stanford, CA 94305, USA*

²*National Institute of Standards and Technology, Physics Laboratory*

100 Bureau Drive, MS 8423, Gaithersburg, MD 20899, USA

³*Paul-Drude-Institut für Festkörperelektronik,*

Hausvogteiplatz 5-7, D-10117 Berlin, Germany and

⁴*National Institute of Informatics, Hitotsubashi, Chiyoda-ku, Tokyo 101-8430, Japan*

Abstract

We perform a Young's double-slit experiment to study the spatial coherence properties of a two-dimensional Bose-Einstein condensate of semiconductor microcavity polaritons. The coherence length of the system is measured as a function of the pump rate, which confirms a spontaneous build-up of macroscopic coherence at the BEC phase transition. An independent measurement reveals that the position and momentum uncertainty product of the condensate is close to the Heisenburg limit. An experimental realization of such a minimum uncertainty wavepacket of the polariton condensate opens a door to coherent matter-wave phenomena such as Josephson oscillation, superfluidity, and solitons in solid state systems.

Simple, yet profoundly connected to the foundation of quantum physics, the Young's double-slit experiment has been used as a benchmark demonstration of macroscopic spatial coherence, i.e., off-diagonal long range order of macroscopic number of particles [1], in Bose-Einstein Condensation (BEC) of cold atoms [2, 3, 4]. Recently, strong evidence of a BEC phase transition has been reported for the lower branch of exciton-polaritons (LPs), in planar semiconductor microcavities [5, 6, 7, 8, 9, 10, 11, 12]. Supporting theoretical frameworks have also been developed [13, 14, 15, 16, 17, 18, 19]. Interestingly, LPs are free particles in a two dimensional (2D) system, but in 2D, genuine BEC exists only at zero temperature if the system size is infinite [20, 21]. A quasi-BEC can be defined in 2D for a system of a finite size if a macroscopic number of particles occupy a single ground state and if an off-diagonal long range order is established throughout the system [22, 23]. Yet in the LP experiments to date, the system size is rather ambiguously defined by the spot size of the pump laser beam, and there is no quantitative study of the relation between the condensate size and its coherence length. In this work, we perform a Young's double slit experiment on a LP gas to measure its spatial coherence properties across the BEC phase transition, and compare the measured coherence length with the condensate size. We also independently measure the momentum uncertainties of the LPs, and compare the position-momentum uncertainty product to the Heisenberg limit.

A sketch of the setup is shown in Fig. 1. The microcavity sample is first magnified by a factor of 37.5 and imaged to a plane A. A lens II then images plane A to a plane B. To observe the spatial distribution of the LP emission, we position lens II such that plane B overlaps with a charge-coupled-device (CCD) located at plane C. To perform a double-slit experiment, we place a pair of rectangular slits at plane A, and position lens II such that the image plane B is a distance D behind plane C. Effectively, we observe on the CCD camera the interference pattern of the LP emission passing through the double-slit. In our experiment, $D = 6.7$ cm, the width of the slit image at plane B is $\delta = 53 \mu\text{m}$, and the average wavelength of the LP emission is $\lambda \sim 778.5$ nm. Correspondingly, the Fresnel number $\frac{\delta^2}{D\lambda} = 0.05 \ll 1$, thus the far-field condition is satisfied at plane C. When mapped onto the sample surface, the slit width seen by the LPs is $\Delta r \approx 0.5 \mu\text{m}$. Δr is less than the intrinsic coherence length $\xi_0 \sim 1.8 \mu\text{m}$ of a single

LP [24], and much less than the LP system size of $5 - 10\mu\text{m}$. Hence neglecting the variation in LP distribution within each slit, we obtain the intensity distribution on the CCD camera at plane C:

$$\begin{aligned}
I(x) &= I_1(x) + I_2(x) + g^{(1)}(|r_1 - r_2|) \cdot 2\sqrt{I_1(x)I_2(x)} \cos(\phi(x) + \phi_{12}), \quad (1) \\
I_i(x) &= |E(r_i)|^2 \cdot \text{sinc}\left(\frac{x - x_0 \pm d/2}{X}\right) \\
\phi(x) &= \frac{2(x - x_0)}{X_c} \\
X &= \frac{2D}{k_{tot}\delta}, \quad X_c = \frac{2D}{kd}.
\end{aligned}$$

The subscript i denotes the slit number, $i = 1, 2$. r_i are the coordinates of the slits on plane B, x is the coordinate on plane C, $E(r_i)$ is the LP field amplitude at slit i , k_{tot} is the free space average wavenumber of the LP emission, and d is the magnified distance between the two slit images at place B. I_i is the intensity distribution if only slit i is open. ϕ_{12} is a fixed phase difference of LPs between the two slits. $\phi(x)$ is a varying phase close to the path length difference from the two slits, which gives rise to a cosine modulation on the far-field intensity distribution. After proper normalization, the amplitude of the cosine modulation equals the first order coherence function $g^{(1)}(r)$. Using six sets of double-slit with varying slit separations r , we measured $g^{(1)}(r)$ from $1.3\ \mu\text{m}$ which is close to the intrinsic coherence length of a single LP up to $8\ \mu\text{m}$ which is close to the LP system size. By varying the pumping intensity, we studied the characteristics of $g^{(1)}(r)$ across the BEC phase transition.

The sample we investigated has a $\lambda/2$ GaAs cavity sandwiched between $\text{Ga}_{0.865}\text{Al}_{0.135}\text{As}/\text{AlAs}$ distributed Bragg reflectors. Twelve quantum wells (QWs) in three stacks are placed at the central three antinodes of the microcavity. We pump the sample with linearly polarized pico-second mode-locked Ti-Sapphire laser. At an incidence angle of 50° from the sample growth direction, the laser pumps resonantly the corresponding exciton-like LP modes. In all experiments, the sample is kept at $T_{lattice} \approx 4\ \text{K}$. The cavity-photon energy at zero in-plane wavenumber is $\sim 7\ \text{meV}$ above the bare QW exciton resonance, corresponding to an optimal detuning for thermal-equilibrium condensation of the LPs [12]. The threshold pumping density is $P_{th} \sim 300\ \text{W/cm}^2$ [25].

A typical interference pattern observed at a pump rate above the BEC threshold is shown in Fig. 2A. Distinct interference fringes are readily observed imposed on a sinc function distribution. To obtain $g^{(1)}(r)$, we integrate over a narrow strip along the y-axis (symbols in Fig. 2B) and fit it with Eq. 2, using $g^{(1)}$, ϕ_{12} , $|E_1|$ and $|E_2|$ as free fitting parameters, while x_0 , d , X and X_c are estimated from experimental parameters with a 10% allowed variation. As shown in Fig. 2B, the fitting curve describes the data very well at a pump rate above the BEC threshold. Below the BEC threshold, the interference patterns are barely observable or non-existing; one example is given in Fig. 2C.

In Fig. 3A we show the increase of $g^{(1)}(r_s)$ with the normalized pump rate P/P_{th} for a few slit separations r_s . The first salient feature in Fig. 3A is that, there is a jump in $g^{(1)}(r_s)$ when the pump rate is increased above a critical value. This demonstrates the sudden appearance of macroscopic coherence above the BEC threshold. Another feature is that, the increase of $g^{(1)}(r_s)$ with P/P_{th} is slower at larger r_s . This shows that the macroscopic coherence is built up gradually throughout the pump beam spot size when the phase space density of LPs is increased.

Even at very low pump rates, a finite $g^{(1)}(r_s) \sim 0.15$ is observed for $r_s = 1.3 \mu\text{m}$. This value is consistent with the $g_0^{(1)}(r_s)$ expected for a single LP with an intrinsic coherence length of ξ_0 :

$$g_0^{(1)}(r_s) = \exp\left(-\frac{\pi r_s^2}{\xi_0^2}\right) = 0.19. \quad (2)$$

To study the spatial coherence properties quantitatively, we plot in Fig. 3B how $g^{(1)}(r)$ decays with r . At higher pump rates, $g^{(1)}(r)$ has a larger value and decays more slowly. For a classical Maxwell-Boltzmann (MB) gas in thermal equilibrium, $g^{(1)}(r)$ decays as

$$g^{(1)}(r) = e^{-\pi r^2/\Lambda_T^2}, \quad (3)$$

$$\Lambda_T = \frac{2\pi\hbar^2}{mk_B T}. \quad (4)$$

Here Λ_T is the thermal de Broglie wavelength, m is the mass of the particles and T is temperature. Fitting of the data with this function is quite poor above the BEC threshold (dashed lines in Fig. 3B).

Since $g^{(1)}(r)$ is the Fourier transform of the momentum distribution $f(k)$, we resort to the actual momentum distribution of the system. It was found that above the BEC threshold, the LPs become highly degenerate in the states with the lowest kinetic energies [9, 12]. Their momentum distribution can no longer be modeled by MB distribution, but follows well the Bose-Einstein (BE) distributions with chemical potential $|\mu| \ll k_B T$. In this limit, $f(E \sim k_B T) = [\exp(\frac{E-\mu}{k_B T}) - 1]^{-1} \approx (e-1)^{-1} \ll f(0) \approx k_B T/\mu$, most of the emission comes from LPs with $E \sim 0$. Hence we can obtain the following approximate form of $g^{(1)}(r)$:

$$\begin{aligned} g^{(1)}(r) &\propto \mathcal{F}^{(2D)}(f(k)g(k)) \propto \mathcal{H}(f(k)) \\ &\approx \mathcal{H}\left(\frac{k_B T}{E(k) - \mu}\right) \\ &\propto K_0\left(r \frac{\sqrt{4\pi|\mu|/k_B T}}{\Lambda_T}\right). \end{aligned} \quad (5)$$

Here k is the LP's in-plane wavenumber, $\mathcal{F}^{(2D)}(f(k))$ and $\mathcal{H}(f(k))$ denote the 2D Fourier transform and Hankel transform of $f(k)$, respectively. $g(k)$ is the constant momentum density of state, and Λ_T is the thermal de Broglie wavelength of the LPs. As shown in Fig. 3B (solid lines), $K_0(x)$, the modified Bessel function of the first kind, fits very well the measured $g^{(1)}(r)$ for $P/P_{th} > 1$.

To compare directly with the momentum distribution, we define r_c as the coherence length, corresponding to the length scale when $g^{(1)}(r)$ decays to $1/e$, i.e., $g^{(1)}(r_c) = 1/e$. We compare in Fig. 4A the pump rate dependence of r_c and Δk (the $1/e$ width of the momentum distribution function $f(k)$), both obtained by spline interpolation of the data. At pump rates lower than the BEC threshold, r_c is $\sim 1 \mu\text{m}$, limited by the intrinsic coherence length ξ_0 of a single LP, while Δk is $\sim 2\mu\text{m}^{-1}$ due to the slow energy relaxation dynamics of the LPs. The product $r_c \cdot \Delta k$ is close to 2, the value expected for a thermal MB distribution. When the pump rate increases toward the threshold, more injected LPs relax to the lower energy states and Δk gradually narrows, but r_c is still limited by ξ_0 , hence a decrease in $r_c \cdot \Delta k$. Once above the threshold, there is a sudden increase of r_c by more than five fold up to $\sim 6 \mu\text{m}$, which manifests the spontaneous build-up of a global phase among the LPs due to the phase coherent stimulated scattering of LPs into the ground state. Correspondingly, Δk is reduced by about four fold since the LPs form

a quantum degenerate Bose gas. Further increasing the pump rates, r_c decrease slightly while the momentum distribution is broadened, potentially because stronger LP-LP scattering at high densities introduces condensate dephasing (self-phase modulation) [19].

Finally, it is instructive to compare Δk with the condensate size measured by imaging the LP emission [9]. We have consistently observed an abnormally slow increase of the condensate size in comparison to the spot size of a photon laser based on electron-hole pairs (Fig. 4C in Ref. [9]).

Due to the discrete jump in quantum efficiency at the BEC threshold (Fig. 2 in Ref. [9]), the emission is much brighter in a condensate region. Since the pump beam has a Gaussian spatial profile, the center of the spot reaches a threshold first, leading to a sharp decrease of the $1/e$ emission spot size ω at P_{th} , for both a LP BEC and a photon laser. At $P > P_{th}$, ω measures the area which reaches the threshold. In a photon laser, ω is determined by the local density of electron-hole pairs. Hence the threshold density is independent of the system size, and ω is given by:

$$\omega(P/P_{th}) = \omega_p \sqrt{1 - \ln(1 + \frac{P}{P_{th}})}, \quad (6)$$

where ω_p is the pump spot size. Eq. 6 describes very well the photon laser data (Fig. 4C in Ref. [9]), but fails to explain the data of a LP condensate (Ref. [9] and Fig. 4B). Here we propose that for a LP condensate, $\omega(P/P_{th})$ reflects the size of the condensate in which a BEC threshold is satisfied. Then the critical LP density $n_c(\omega)$ increases with the system size ω , and Eq. 6 needs to be modified as:

$$\omega(P/P_{th}) = \omega_p \sqrt{1 - \ln(1 + \frac{P}{P_{th}} \frac{n_c(\omega(P/P_{th}))}{n_c(\omega_c)})}, \quad (7)$$

where ω_c is the condensate size at $P = P_{th}$. As a simplified model, consider n_c for a 2D boson gas confined in a finite size $L = 2\omega$ [26]:

$$n_c(\omega) = \frac{2}{\Lambda_T^2} \ln(\frac{2\omega}{\Lambda_T}), \quad (8)$$

Substitute Eq. 8 to 7, we obtain:

$$\omega(P/P_{th}) = \omega_p \sqrt{1 - \ln(1 + \frac{P}{P_{th}} \frac{\ln(2\omega/\Lambda_T)}{\ln(2\omega_c/\Lambda_T)})}. \quad (9)$$

Using ω_p and ω_c as fitting parameters, Eq. 9 fits the data very well (solid line in Fig. 4B). This result suggests that the slow increase of the observed spot size could be another signature of LP BEC, and 2ω measures the size of the coherent condensate above threshold.

With the distribution functions in both spatial and momentum domains, we can evaluate how well the system can be described by a single-particle wavefunction. The standard deviation σ_k and σ_r are calculated from the momentum and spatial distribution data $f(k)$ and $f(r)$ at $P > P_{th}$, respectively; their product is compared to the Heisenberg minimum uncertainty limit in Fig. 4C. The sharp decrease of $\sigma_k \cdot \sigma_r$ at $P \sim P_{th}$ indicates that a large number of the LPs in the system condense into a single quantum state. Deviation from the Heisenberg limit shows that there are some thermal LPs coexisting with the coherent condensate. The slight increase of $\sigma_k \cdot \sigma_r$ at $P/P_{th} > 1$ may be caused by condensate depletion due to LP-LP interactions at high densities [19, 27].

In conclusion, we studied the spatial coherence of a Bose-Einstein Condensate of microcavity polaritons. A Young's double-slit setup is implemented to measure the first order coherence function $g^{(1)}(r)$ of the LPs. The system acquires macroscopic coherence above a BEC threshold, manifested as a sudden jump of $g^{(1)}(r)$. The coherence length r_c grows with further increasing pump rates. The observed $g^{(1)}(r)$ vs. r is well described by the Fourier transform of a degenerate Bose-Einstein distribution in the momentum space. The increase of the coherence length is consistent with the narrowing of the momentum space distribution measured independently. The coherent condensate expands from the central region of the pump spot to the full pump spot size, and a slow growth of the condensate size is well understood by a simple model of BEC with a finite size. Consistent with a long range but finite coherence length, the uncertainty product $\sigma_k \sigma_r$ of the LPs decreases toward the Heisenberg uncertainty limit above a BEC threshold.

The authors thank C.W. Lai and N.Y. Kim at Stanford University for their useful comments. This research is supported by the Quantum Entanglement Project, SORST, JST.

-
- [1] O. Penrose and L. Onsager, Phys. Rev. **104**, 576 (1956).
 - [2] M. R. Andrews, C. G. Townsend, H.-J. Miesner, D. S. Durfee, D. M. Kurn, and W. Ketterle, Science **275**, 637 (1997).
 - [3] I. Bloch, T. W. Hänsch, and T. Esslinger, Nature **403**, 166 (2000).
 - [4] Z. Hadzibabic, P. Krger, M. Cheneau, B. Battelier, and J. Dalibard, Nature **441**, 1118 (2006).
 - [5] L. S. Dang, D. Heger, R. André, F. Boeuf, and R. Romestain, Phys. Rev. Lett. **81**, 3920 (1998).
 - [6] P. Senellart and J. Bloch, Phys. Rev. Lett. **82**, 1233 (1999).
 - [7] R. Huang, Y. Yamamoto, R. André, J. Bleuse, M. Muller, and H. Ulmer-Tuffigo, Phys. Rev. B. **65**, 165314 (2002).
 - [8] H. Deng, G. Weihs, C. Santori, J. Bloch, and Y. Yamamoto, Science **298**, 199 (2002).
 - [9] H. Deng, G. Weihs, D. Snoke, J. Bloch, and Y. Yamamoto, Proc. Natl. Acad. Sci. **100**, 15318 (2003).
 - [10] M. Richard, J. Kasprzak, R. Romestain, R. Andre, and L. S. Dang, Phys. Rev. Lett. **94**, 187401 (2005).
 - [11] J. Kasprzak, M. Richard, S. Kundermann, A. Baas, P. Jeambrun, J. M. J. Keeling, F. M. Marchetti, M. H. Szymaska, R. Andr, J. L. Staehli, et al., Nature **443**, 409 (2006).
 - [12] H. Deng, D. Press, S. Götzinger, S. G., H. R., K. Ploog, and Y. Yamamoto, Phys. Rev. Lett. **97** (2006).
 - [13] P. Littlewood, P. Eastham, J. Keeling, F. Marchetti, and M. Szymanska, J. Phys.: Cond. Matt. **16**, S3597 (2004), and refereces therein.
 - [14] J. Keeling, F. M. Marchetti, M. H. Szymanska, and P. B. Littlewood (2007), (Available at <http://arxiv.org/abs/cond-mat/0702166>).
 - [15] G. Malpuech, Y. Rubo, F. Laussy, P. Bigenwald, and A. Kavokin, Semicond. Sci. Technol. **18**, S395 (2003).
 - [16] K. Kavokin, I. Shelykh, A. Kavokin, G. Malpuech, and P. Bigenwald, Phys. Rev. Lett. **92**, 017401 (2004).

- [17] H. Cao, T. Doan, D. Thoai, and H. Haug, *Phy. Rev. B* **69**, 245325 (2004).
- [18] T. D. Doan, H. T. Cao, D. Thoai, and H. Haug, *Phys. Rev. B* **72**, 85301 (2005).
- [19] D. Sarchi and V. Savona (2006), (Available at <http://arxiv.org/abs/cond-mat/0603106>).
- [20] N. D. Mermin and H. Wagner, *Phys. Rev. Lett.* **17**, 1133 (1966), erratum: *PRL*, Vol. 17, No.26, 12/26/66.
- [21] P. Hohenberg, *Physical Review* **158**, 383 (1967).
- [22] V. Bagnato and D. Kleppner, *Phys. Rev. A* **44**, 7439 (1991).
- [23] J. Lauwers, A. Verbeure, and V. A. Zagrebnov, *Journal of Physics, A* **36**, L169 (2003).
- [24] The coherence length ξ_0 of a single LP is defined by the Fourier transform of the LP's far field radiation pattern, and is calculated by a transfer matrix method. A detailed procedure is given in G. Bjork, S. Machida, Y. Yamamoto and K. Igeta, *Phy. Rev. A* **44**, 669 (1991).
- [25] The operational threshold is defined at the steepest slope of the input-output curve for LPs at $k = 0$.
- [26] W. Ketterle and N. J. van Druten, *Phys. Rev. A* **54**, 656 (1996).
- [27] C. Orzel, A. K. Tuchman, M. L. Fenselau, M. Yasuda, and M. A. Kasevich, *Science* **291**, 2386 (2001).

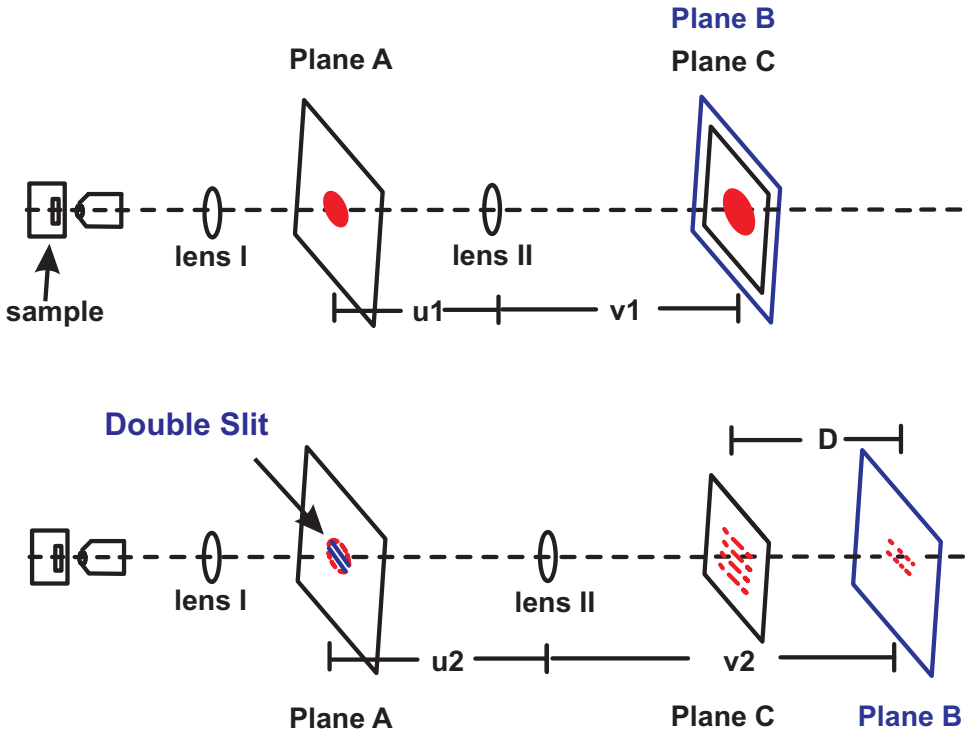


FIG. 1: A sketch of the double-slit experiment setup. In the upper configuration, the LP spatial distribution is imaged to a CCD camera at plane C. In the lower configuration, a double-slit is inserted at plane A and imaged by lens II to a virtual plane B. The CCD camera at plane C, a distance D from plane B, captures the double-slit interference pattern.

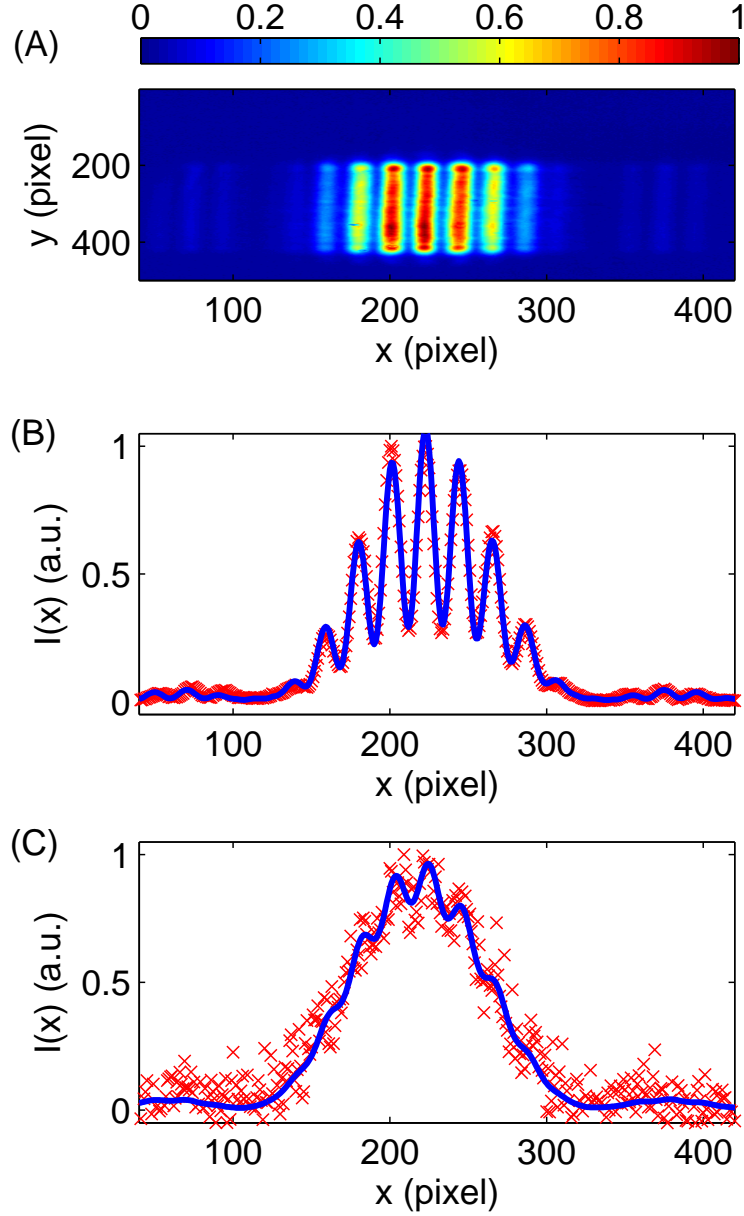


FIG. 2: **(A)** Raw image of the interference pattern, slit separation $r_2 = 2.7 \mu\text{m}$, $P/P_{th} = 7$. **(B)** Measured (symbols) intensity $I(x)$ for $r_2 = 2.7 \mu\text{m}$, $P/P_{th}=7$ and fitting by Eq. 2. Fitted $g^{(1)}(r_2) = 0.560 \pm 0.006$. **(C)** Same as (B), for $r_2 = 2.7 \mu\text{m}$, $P/P_{th} = 0.5$ and $g^{(1)}(r_2) = 0.09 \pm 0.02$.

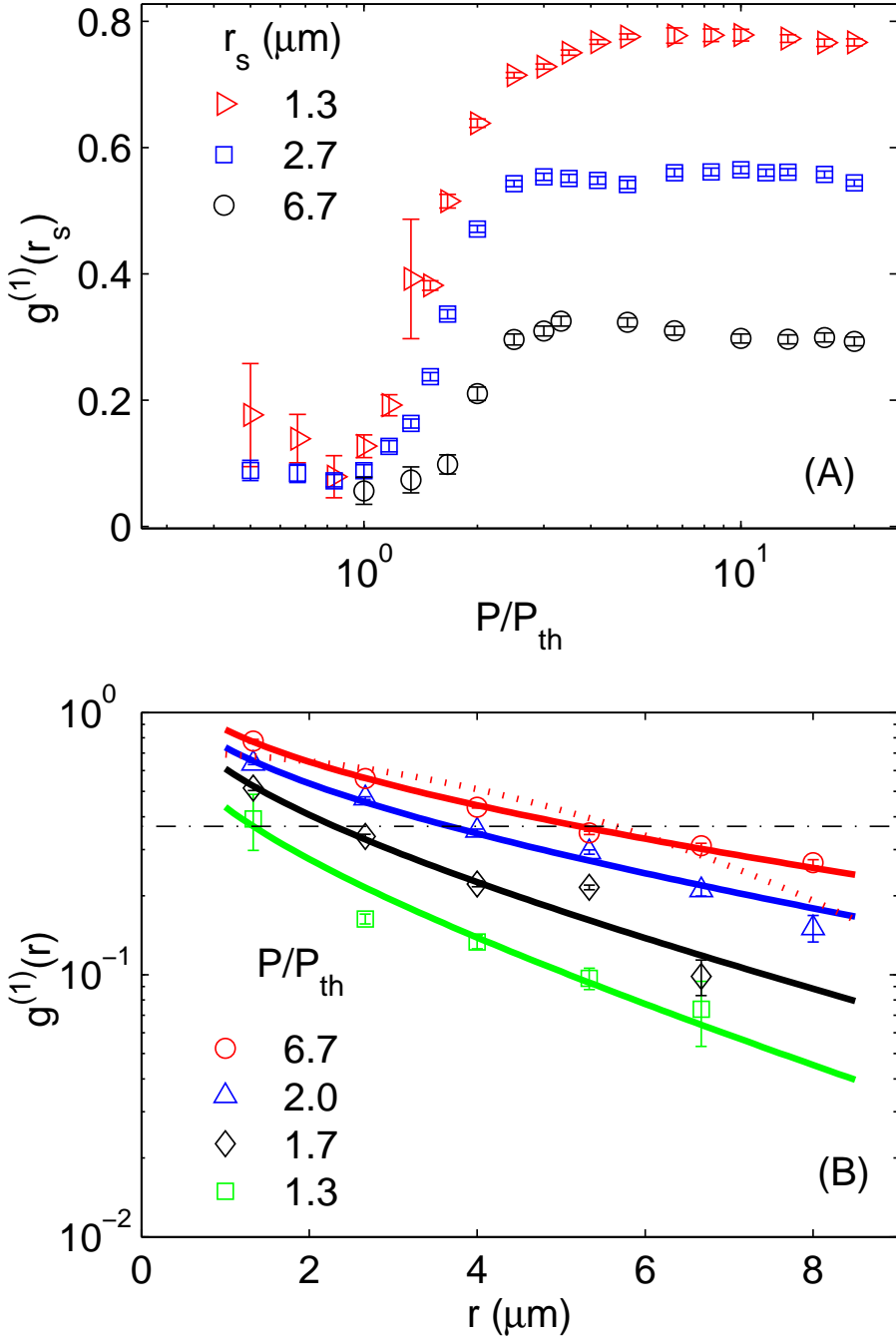


FIG. 3: (A) $g^{(1)}(r_s)$ vs. P/P_{th} for different slit separations r_s as labeled in the figure. (B) $g^{(1)}(r)$ vs. r for different pump rates P/P_{th} as given in the legend. The symbols are measured $g^{(1)}(r)$. The solid lines are fittings by Eq. 5. The dashed line at $P/P_{th} = 7$ is a fitting by Eq. 3.

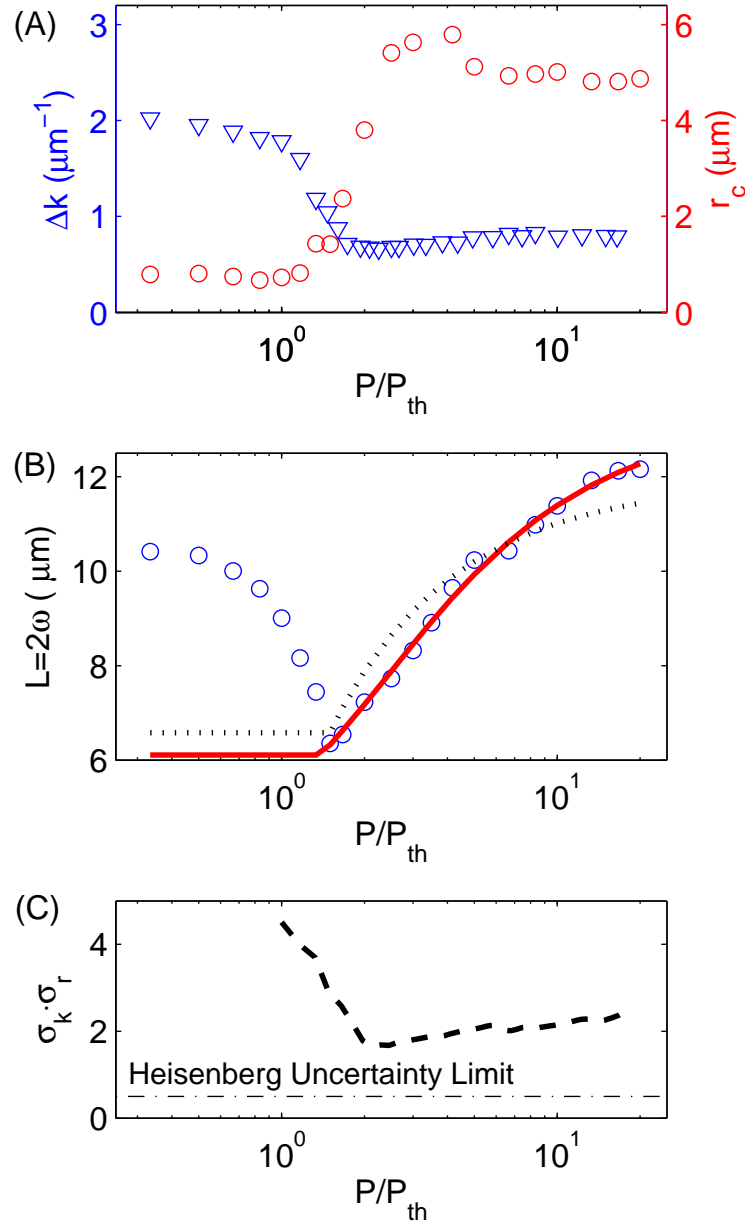


FIG. 4: (A) Δk vs. P/P_{th} (left axis) and r_c vs. P/P_{th} (right axis). (B) System size 2ω vs. pump rates P/P_{th} . Symbols are the data. The solid line is a fitting by Eq. 9, with $\omega_p = 13.3 \pm 0.1 \mu\text{m}$, $\omega_c = 6.1 \pm 0.1 \mu\text{m}$. The dotted line is a fitting by Eq. 6 for comparison, with $\omega_p = 11.9 \pm 0.02 \mu\text{m}$. (C) The position and momentum uncertainty product $\sigma_k \cdot \sigma_r$ vs. P/P_{th} . The dash-dotted line indicates the minimum uncertainty of $\sigma_k \cdot \sigma_r = 1/2$.